# Bipolar membranes for intrinsically stable and scalable CO2 electrolysis

Petrov K.V.; Koopman, C.I.; Subramanian, S.; Koper, M.T.M.; Burdyny, T.; Vermaas, D.A.

nature energy

Perspective

https://doi.org/10.1038/s41560-024-01574-y

# Bipolar membranes for intrinsically stable and scalable $CO_2$ electrolysis

Received: 3 August 2023

Accepted: 6 June 2024

Published online: 24 July 2024

Check for updates

Kostadin V. Petrov[1,3], Christel I. Koopman[1,3], Siddhartha Subramanian[1], Marc T. M. Koper[2] ✉, Thomas Burdyny[1] ✉ & David A. Vermaas[1] ✉

$CO_2$ electrolysis allows the sustainable production of carbon-based fuels and chemicals. However, state-of-the-art $CO_2$ electrolysers employing anion exchange membranes (AEMs) suffer from (bi)carbonate crossover, causing low $CO_2$ utilization and limiting anode choices to those based on precious metals. Here we argue that bipolar membranes (BPMs) could become the primary option for intrinsically stable and efficient $CO_2$ electrolysis without the use of scarce metals. Although both reverse- and forward-bias BPMs can inhibit $CO_2$ crossover, forward-bias BPMs fail to solve the rare-earth metals requirement at the anode. Unfortunately, reverse-bias BPM systems presently exhibit comparatively lower Faradaic efficiencies and higher cell voltages than AEM-based systems. We argue that these performance challenges can be overcome by focusing research on optimizing the catalyst, reaction microenvironment and alkali cation availability. Furthermore, BPMs can be improved by using thinner layers and a suitable water dissociation catalyst, thus alleviating core remaining challenges in $CO_2$ electrolysis to bring this technology to the industrial scale.

Electrochemical $CO_2$ reduction ($CO_2R$) is a promising technology for the production of sustainable carbon-based fuels and chemicals. Having reached current densities and Faradaic efficiencies that are near commercial standards, critical parameters of interest are now stability, energy efficiency, $CO_2$ utilization and material availability. As a modulator of the ionic current and a separator of $CO_2$ conversion at the cathode and the oxygen evolution reaction (OER) at the anode, the ion exchange membrane plays a central role in the performance, material selection and stability of the configuration.

Currently, the most efficient and high-performing $CO_2$ electrolysers employ anion exchange membranes (AEMs) in a membrane electrode assembly configuration (Fig. 1a). Ideally, the AEM facilitates the selective transport of hydroxide ions ($OH^-$) from the cathode to the anode. However, AEM-based electrolysers face a major challenge since a large part of the input $CO_2$ reacts with $OH^-$ to produce (bi) carbonates, which are then transported to the anode compartment through the AEM[1].

To properly assess the industrial feasibility of AEM-based systems, we need to include the implications of $CO_2$ crossover on the energy and material requirements. The crossover of $CO_2$ in the form of (bi) carbonates means that an alkaline environment at the anode cannot be maintained without electrolyte regeneration. At the same time, the only high-performing OER catalyst under neutral (or acidic) conditions is Ir, thus implying that AEM-based systems necessitate the use of iridium-based catalyst at the anode[2]. However, iridium is one of the scarcest metals on Earth and its rising price is an impediment for scale-up[3]. Moreover, $CO_2$ crossover limits the (single-pass) $CO_2$ utilization to 50% or lower depending on the product (for CO, 50%; for $C_2H_4$, 25%)[4]. Given that producing a concentrated $CO_2$ feed requires energy (conventional $CO_2$ capture processes have an energy consumption between 170 and 390 kJ $mol^{-1}$ $CO_2$, depending on the source of $CO_2$[5,6]) incomplete $CO_2$ utilization can be considered an indirect energy penalty. For example, an energy consumption of 170 kJ $mol^{-1}$ $CO_2$ would translate to a voltage of 0.88 V when recapturing $CO_2$ from the anode gas (assuming 100% Faradaic efficiency and $CO_3^{2-}$ as the charge carrier). Hence, increasing the $CO_2$ utilization is a necessity for a scalable and efficient $CO_2$ electrolysis technology.

An alternative to AEMs to address these issues is the use of bipolar membranes (BPMs). BPMs consist of a cation exchange layer (CEL) and an anion exchange layer (AEL) and, depending on the

[1]Chemical Engineering Department, Delft, the Netherlands. [2]Leiden Institute of Chemistry, Leiden University, Leiden, the Netherlands. [3]These authors contributed equally: Kostadin V. Petrov, Christel I. Koopman. ✉e-mail: m.koper@chem.leidenuniv.nl; t.e.burdyny@tudelft.nl; d.a.vermaas@tudelft.nl

https://doi.org/10.1038/s41560-024-01574-y

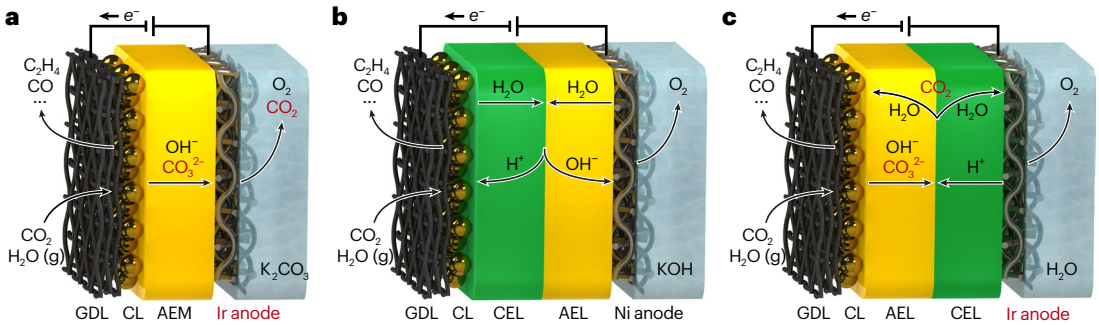


**Fig. 1 | Cell configurations for electrochemical $CO_2R$. a–c**, Three potential cell configurations for electrochemical $CO_2R$, including an AEM electrode assembly (**a**), a BPM electrode assembly in reverse-bias configuration (**b**) and a BPM electrode assembly in forward-bias configuration (**c**). All of the configurations are equipped with a GDE paired with oxygen evolution at the anode in a liquid anolyte. The GDE consists of a gas diffusion layer (GDL) and a catalyst layer (CL). All species except for $H_2O$ (g) in the gas channel are in the standard phase (at room temperature). Species displayed in red indicate undesired crossover or use of scarce materials.

orientation, can be used in forward- or reverse-bias configuration. In reverse-bias configuration (Fig. 1b), water dissociates into $H^+$ and $OH^-$ at the CEL/AEL interface. The $H^+$ migrates to the cathode and the $OH^-$ migrates to the anode, while (theoretically) no other ions can pass both layers of the BPM. Combined with proton-coupled electron transfer reactions, such as $CO_2R$ and OER, the BPM theoretically produces or consumes $H^+$ and $OH^-$ at the same rate as the production/consumption at the electrodes, allowing operation at a steady-state pH difference between the electrodes. This offers the benefit of a theoretically stable alkaline anolyte, which is favourable for the OER and allows the use of more Earth-abundant catalysts such as NiFeOx[7]. Moreover, the CEL rejects carbonates and the generated $H^+$ recombines with carbonates to regenerate $CO_2$, impeding $CO_2$ crossover almost entirely.

However, a current bottleneck for reverse-bias BPMs is that the resulting acidic cathode environment has been associated with low Faradaic efficiencies for $CO_2R$ products, since the competitive $H_2$ evolution reaction (HER) is promoted in the abundance of $H^+$ (ref. 8). Fortunately, recent advances have been made in $CO_2R$ in acidic media and the impact of cations on $CO_2R$ is now better understood, offering strategies for suppressing the HER, providing interesting opportunities for reverse-bias BPM systems[9–11]. Conversely, an ideal forward-bias BPM (Fig. 1c), where $OH^-$ from the cathode migrates through the adjacent AEL and recombines with $H^+$ from the anode, enables a neutral/alkaline environment at the cathode, but fails to provide anode conditions that permit the use of Earth-abundant catalysts.

In this Perspective, we argue that BPMs have the potential to be the primary option for $CO_2$ electrolysis, as AEMs cannot prevent $CO_2$ crossover and the associated adverse energy and material implications that come with it. We assess the potential of BPMs for $CO_2$ electrolysis, with special attention to $CO_2$ utilization, energy consumption and strategies to improve product selectivity and efficiency. We conclude that for BPMs to be the new state-of-the-art option, their performance—in terms of conductance, BPM kinetics and stability—must be improved through innovation.

## BPMs promote $CO_2$ utilization by inhibiting crossover

The $CO_2$ crossover in AEM-based $CO_2$ electrolysers proves to be an intrinsic limitation. Typically, AEM-based systems exhibit a crossover of between 0.5 and 1.0 $CO_2$ per $e^-$ transferred, which corresponds to $CO_3^{2-}$ and $HCO_3^-$ as the dominant charge carriers, respectively (Fig. 2a). Therefore, to achieve higher $CO_2$ utilization, (bi)carbonate formation/crossover must be suppressed, which can—with currently known materials—only be done by replacing AEM separators with either a BPM or a cation exchange membrane (CEM)[12–14].

$CO_2$ crossover is heavily decreased for BPM-based systems (Fig. 2a,b) due to the presence of negatively charged groups in the CEL, which inhibits $CO_2$ crossover through Donnan exclusion of carbonates and negatively charged $CO_2R$ products (formate)[15]. We note that some crossover of co-ions can occur through uncharged membrane spaces (between charged phases)[16], but this issue is minor given the typical water dissociation efficiency of >99% at 100 mA $cm^2$, and is manageable using existing strategies against salt precipitation and electrolyte regeneration[17]. Additionally, reverse-bias BPMs decrease the crossover of neutral $CO_2R$ products (for example, methanol) through the outward flux of protons, which inhibits electro-osmotic drag across the membrane, in particular at higher current densities (Fig. 2b)[18].

Although CEM-based electrolysers are able to achieve low $CO_2$ crossover, they are more prone to instabilities due to co-ion crossover. Furthermore, their acidic/neutral anolyte conditions require the use of scarce metals, making the BPM-based system a more suitable candidate for large-scale application[3,13].

BPM-based systems in either the reverse- or forward-bias configuration have been reported that achieve high single-pass $CO_2$ utilization values of up to 78%[13,19], surpassing the theoretical maximum of 50% for AEM-based systems for two-electron products[12]. The typical 0.02 $CO_2$ lost per electron (Fig. 2b) implies a maximum of 96% $CO_2$ utilization, but high single-pass utilization is still expected to bring about trade-offs in selectivity and energy efficiency through the concentration overpotential caused by reactant starvation[20].

At the moment, the improved $CO_2$ utilization of reverse-bias BPM-based systems comes at the cost of lower Faradaic efficiencies and higher cell voltages (Fig. 2c,d). However, unlike the intrinsic issues of $CO_2$ crossover and the need for scarce metals in anode materials for AEM-based systems, in this Perspective we argue that both the selectivity and cell voltage for BPM-based systems can be further improved through innovation.

## The key to low cell potentials is managing pH gradients

A large contribution to the high voltages observed in BPM and CEM electrolysers, which is often overlooked, stems from pH gradients within the electrolyser. Assuming that an electrolyser is producing CO and $O_2$, the difference between the standard reduction potentials ($E^0_{cell}$) is 1.34 V. Because both reactions produce one $H^+$ or $OH^-$ per electron, each pH unit causes a Nernstian shift of 59.2 mV. Theoretically, the voltage contribution of water dissociation or recombination (0.83 V) at the BPM interface is counter-balanced by the Nernstian shift in redox potential at the electrodes, which would allow all configurations to operate at the same equilibrium cell voltage (1.34 V; see $E^0_{cell}$ in the 'RHE scale' at the bottom of each panel in Fig. 3).

https://doi.org/10.1038/s41560-024-01574-y

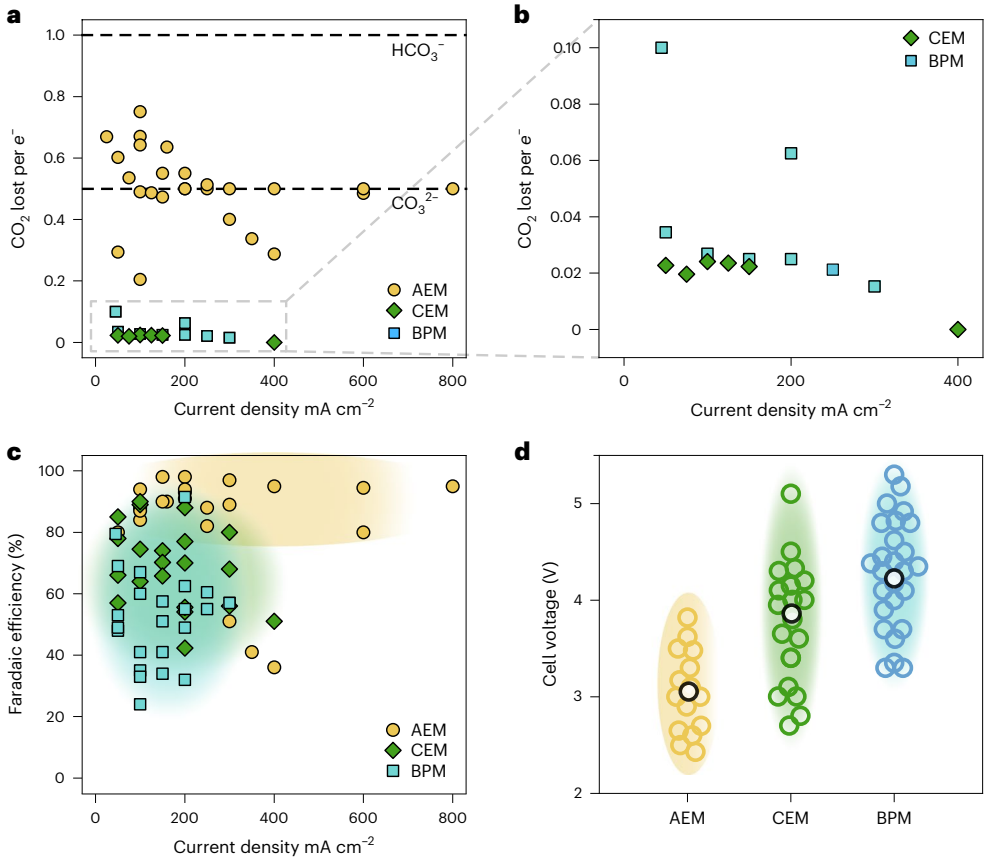


**Fig. 2 | Comparison of performance parameters for AEM-, BPM- and CEM-based $CO_2$ electrolysers. a**,**b**, Relative $CO_2$ crossover per charge transferred. The data points represent values from several studies, whereas the lines represent the theoretical values when $CO_3^{2-}$ or $HCO_3^-$ are the main charge carriers. This assumes one $OH^-$ per reaction electron (valid for most $CO_2R$ reactions and HERs) and no $H_2CO_3$ crossover. The results shown in **b** are a magnification of the section outlined by a dashed box in **a**. **c**, Faradaic efficiency for carbon-based products. **d**, Cell voltages for the different membrane systems at current densities between 50 and 300 mA $cm^{-2}$. The values shown by a white circle outlined in black show the average cell voltage of all of the data points. See Source Data Fig. 2 for underlying data and specific accompanying refs. 2,9,10,12–14,31,34,38,39,49–60.

In practice, however, pH gradients and buffering effects will change the local pH and therefore the observed difference in redox potentials and cell potentials. Accurately determining the pH in the cathode reaction environment remains a challenge for zero-gap configurations. Whereas the catholyte pH is largely controlled by the generated $OH^-$ and carbonate equilibrium constant, the anolyte pH depends on $[K^+]$ and the partial pressure of $CO_2$ in the mixed anode gas. For the sake of this discussion, we assume a cathode pH of 10.5 (close to the carbonate acid dissociation constant ($pK_a$)) and an anolyte pH of 8.1 (equilibrium at 1 M $K^+$ and 0.5 bar partial pressure $CO_2$)[9,21]. Hence, the pH gradient over the AEM increases the cell voltage by at least 0.14 V ($(10.5 - 8.1) \times 0.0592 = 0.14$; Fig. 3a).

In a reverse-bias BPM electrolyser, a large pH gradient is observed between the CEL and the catalyst layer, since the BPM interface produces $H^+$ whereas the produced $OH^-$ and carbonate pin the pH to ~10.5 (Fig. 3b). This gradient does not allow the complete balancing of the water dissociation voltage of 0.83 V. At a cathode pH of 10.5, only 0.21 V is compensated. Operating a cathode at acidic pH would be extremely beneficial for this configuration, since removing the internal pH gradient would lower the overall cell potential by 0.62 V. Additionally, the BPM requires an overpotential for water dissociation and increased ohmic resistance can be caused by the formation of bubbles at the CEL interface[22].

For an electrolyser with a forward-bias BPM (Fig. 3c), the buffering effects occur both in the catalyst layer and at the BPM interface. The Nernstian pH shift added by the alkalinity in the cathode region in this scenario is 0.56 V. The forward-bias BPM electrode assembly configuration could potentially recover this energy at the BPM junction, but recent work[23] shows that the main recombined species is $H_2CO_3$ instead of water, lowering the maximum regained voltage to 0.38 V (derived from $0.0592pK_a(H_2CO_3)$).

## Why forward bias fails to solve $CO_2$ electrolysis challenges

The forward-bias BPM electrode assembly configuration (Fig. 1c) has the advantages of maintaining an alkaline environment at the cathode (which ensures a high Faradaic efficiency) and decreasing $CO_2$ loss without a very high energy penalty. However, in addition to the incomplete recovery of the Nernstian pH shift due to carbonate formation, this configuration has additional challenges. In the forward-bias configuration, the formation of water and gaseous $CO_2$ at the interface of the BPM causes blistering and delamination in commercial BPMs at current densities above 20 mA $cm^2$, thus rendering them ineffective in practice. Additionally, as shown in recent works[23,24], (bi)carbonate ions and weak acids can induce large neutralization overpotentials and the inefficient transport of the produced $CO_2$ leads to low limiting current densities.

Effective removal of $CO_2$ generated at the BPM interface is this essential and future research should address this issue with smart membrane design strategies such as the use of a hybrid liquid–membrane interface or an AEL with a porous or micro-channelled structure[25–27], including successful operation for 200 h[19]. Alternatively, designing BPMs with high selectivity for $OH^-$ ions over co-ions (such as carbonate, formate or acetate) could mitigate ionic blockades and elevate limiting current densities to industrially relevant rates (>100 mA $cm^2$).

https://doi.org/10.1038/s41560-024-01574-y

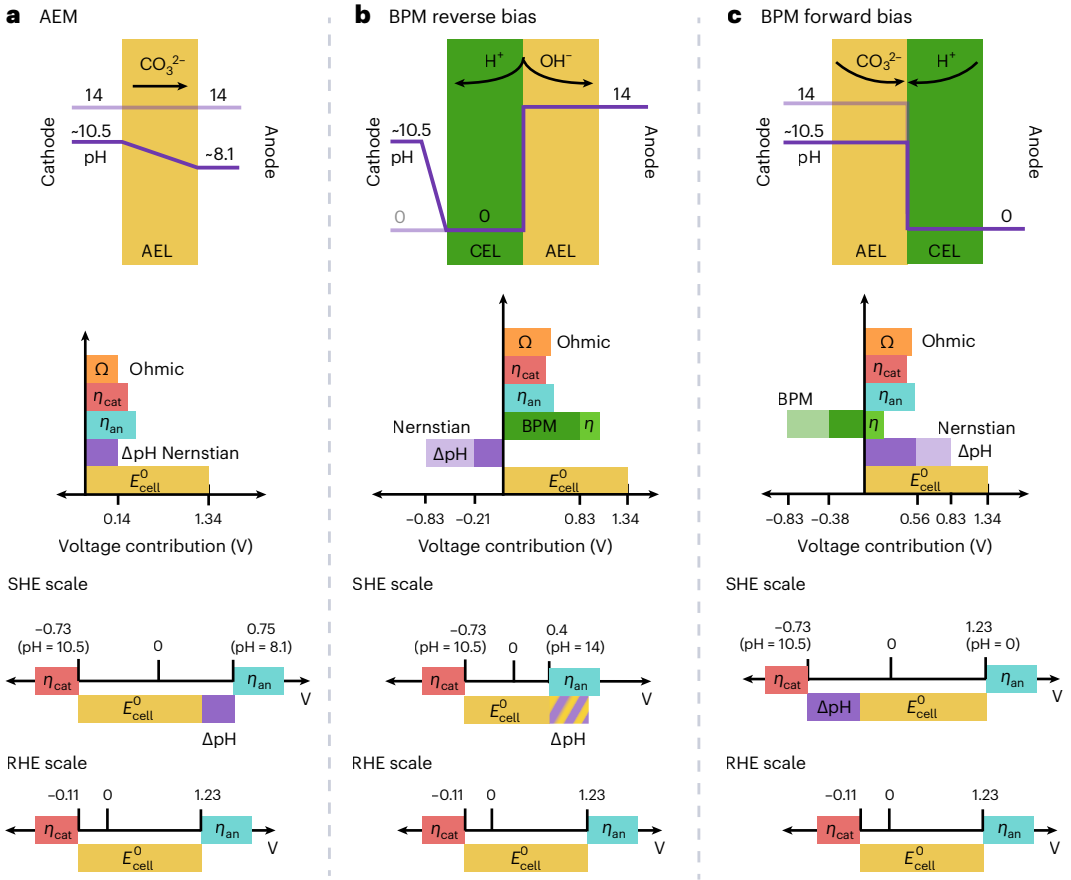


**Fig. 3 | Simplified membrane electrode assembly configurations and the voltage contributions of the different components. a**–**c**, Membrane electrode assembly configurations and voltage contributions for the AEM electrode assembly system (**a**), reverse-bias BPM electrode assembly (**b**) and forward-bias BPM electrode assembly (**c**). Top, pH profiles for ideal case (light purple lines) and realistic conditions (dark purple lines). Middle, $\eta_{an}$ and $\eta_{cat}$ represent the overpotentials of the anode and cathode, respectively, Ω represents the ohmic resistance contribution, $E^0_{cell}$ is the difference between the equilibrium redox potentials of the two reactions, ΔpH Nernstian represents the Nernstian pH shift and BPM is the voltage associated with the water dissociation or recombination reaction at the BPM interface. Contributions for $E^0_{cell}$, ΔpH Nernstian and BPM were calculated (see main text), whereas Ω, $\eta_{an}$ and $\eta_{cat}$ are indicative. The light shaded Nernstian and BPM contributions correspond to the ideal pH profile, whereas the saturated shaded contributions correspond to the realistic pH profile. The voltage contributions of the reactions on the individual electrodes are also displayed on the scales of standard hydrogen electrode (SHE) and reversible hydrogen electrode (RHE) to highlight the effect of pH on the equilibrium redox potentials.

Although blistering and delamination can be overcome by engineering techniques, the forward-bias case suffers from decreased voltage gain due to carbonic acid recombination, unfavourable pH conditions in the anode and the necessity for scarce anode materials, which are difficult to overcome.

## Controlling the BPM microenvironment to promote $CO_2R$

Until recently, the reverse-bias BPM-based membrane electrode assembly showed low Faradaic efficiency due to the acidic microenvironment favouring the HER. However, recent studies have demonstrated that manipulating cation concentrations, ionomer properties and system configuration promotes $CO_2R$ relative to the HER. The presence of alkali cations with small hydrated radii, such as $Cs^+$ and $K^+$, was demonstrated to promote $CO_2R$ even in strong acid[10]. Unlike the HER, which involves proton-coupled electron transfer, the rate-limiting step for $CO_2R$ is the adsorption of $CO_2$ onto the catalyst by cation-coupled electron transfer (the formation of cation-stabilized $CO_2$ adsorbate, $cat^+$-*$CO_2^-$)[28]. Therefore, the cation concentration near the catalyst has an important role in determining $CO_2R$ kinetics[29]. Moreover, since cation-coupled $CO_2R$ is a hydroxide-generating reaction instead of a proton-consuming reaction, it can neutralize incoming protons and thereby suppress the HER from proton reduction[11]. In this way, water reduction is not suppressed, but this reaction happens at more negative potentials. The challenge is controlling the reaction microenvironment (including pH and alkali cations).

We highlight five strategies for controlling the reaction microenvironment to achieve high Faradaic efficiency in reverse-bias configuration. First, introducing a thin alkali cation-rich catholyte layer (Fig. 4a) provides the necessary cations in the vicinity of the catalyst particles, whereas the $H^+$ ions provided by the BPM react with $OH^-$ so that carbonate production is minimized. Xie et al.[13] added a 65 μm thin catholyte layer with 0.5 M $K_2SO_4$ and achieved a Faradaic efficiency for $CO_2R$ products of ~80% at 300 mA $cm^2$.

Similar to the previous strategy, pre-conditioning the BPM with $K^+$ or $Cs^+$ ions (Fig. 4b) would ensure the presence of alkali cations in the vicinity of the catalyst, promoting $CO_2R$. Xiao et al.[30] successfully exchanged the $H^+$ in a Nafion membrane with $Na^+$ or $K^+$ ions, which led to a Faradaic efficiency of CO ($FE_{CO}$) of 91.5% in the initial stage of $CO_2$ electrolysis. The salt deposition problems that occur for the CEM case after 1 h may be resolved when applying this strategy to a BPM, as the supply of new cations is blocked by the AEL.

The third strategy involves employing catalysts that are $CO_2R$ active in acidic media (Fig. 4c). From a theoretical standpoint, a strongly acidic cathodic environment resembles the ideal electrode potentials (Fig. 3b) and warrants high ionic conductivity. Immobilized molecular

https://doi.org/10.1038/s41560-024-01574-y

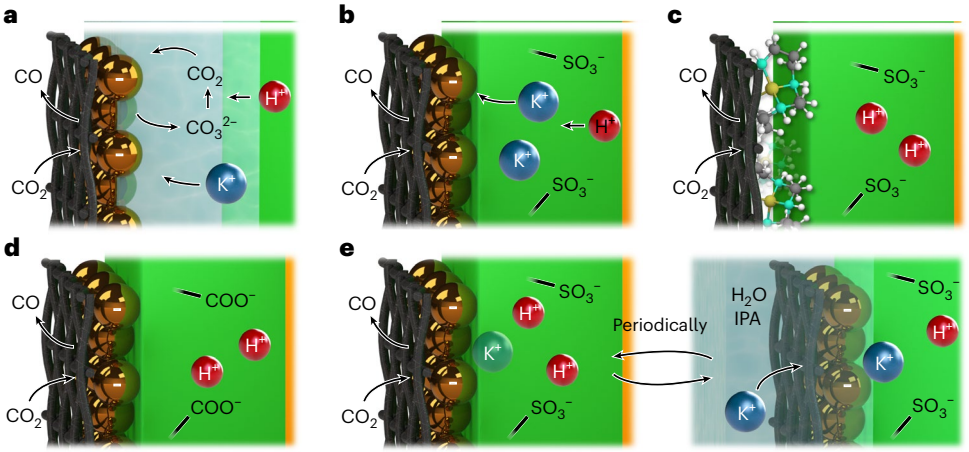


**Fig. 4 | Strategies to alleviate BPM–catalyst interaction. a–e**, Strategies for the alleviation of BPM–catalyst interaction include adding a catholyte layer (**a**), loading the CEL with $K^+$ (**b**), employing $CO_2R$ selective molecular catalysts for acidic media (**c**), using CELs with weakly acidic groups (**d**) or periodically injecting $K^+$ from the back of the GDE with water and isopropanol (IPA) (**e**).

catalysts have the potential to catalyse $CO_2R$ under such acidic conditions. For example, Siritanaratkul et al.[31] used [Ni(1,4,8,11-tetraazacyclotetradecane)]$^{2+}$ to achieve 40% higher $FE_{CO}$ compared with an Ag catalyst in a zero-gap reverse-bias configuration. Also, co-depositing Lewis acids, which are proven for local pH tuning in seawater electrolysis[32], is inspiring in modification of the local environment in $CO_2R$.

The fourth strategy leverages weak acids to decrease the acidity in the reaction microenvironment (Fig. 4d). Weak acidic groups decrease the membrane charge at low pH and thus the $H^+$ concentration. Using alternating poly(acrylic acid) and poly(allylamine hydrochloride) as weakly acidic groups in the CEL demonstrated an increased $FE_{CO}$ (40%)[33]. When further optimizing this strategy, it must be considered that the near-neutral pH will shift the cathode potential (Fig. 3b). Theoretically, the water dissociation could occur at <0.83 V if the $H^+$ concentration in the CEL is <1 M, but it seems unlikely to fully compensate for the cathode potential shift (for example, pH 4 would imply $[H^+]$ = 0.1 mM, which would cause transport limitations in the CEL).

The final strategy is the periodic injection of cations from the back of the gas diffusion electrode (GDE; Fig. 4e). This strategy has not been applied to BPM-based electrolysers, but Endrődi et al.[34] supplied $Cs^+$ ions (isopropanol/water with 1 M CsOH) every 12 h and achieved stable operation in an AEM electrode assembly electrolyser (~90% $FE_{CO}$ for over 200 h).

The first strategy is the most simple and has proven efficacy at small scales[13]. However, introducing a catholyte layer can pose engineering challenges during scale-up related to GDE breakthrough or flooding and the formation of $CO_2$ gas bubbles near the BPM[13,35]. The second and fourth strategy can also be applied on the ionomers often used in the catalyst layer to modify the reaction microenvironment. Strategies that ensure the presence of cations (first, second and fifth) could be largely affected by water evaporation at the GDE, causing the cations to be removed as aerosols in the product stream and compromising the electrolyser stability. To minimize cation loss, the humidity of the $CO_2$ gas stream, the process temperature and cation crossover (required at small rates to replenish cations) are key parameters to optimize.

The third strategy, which involves using catalysts active in acidic media, has the added promise of decreasing the cell potential by mitigating the pH gradient between the CEL and catalyst layer. However, such catalysts are in an early stage of development and face challenges such as deactivation by CO and degradation[31]. Nevertheless, we would urge the electrocatalysis field to focus more efforts in this direction, since a stable $CO_2R$ catalyst that operates in acidic media would solve both main challenges associated with reverse-bias BPM operation.

## Outlook

Parameters known to optimize BPMs are conductivity, water dissociation kinetics, water permeability, lifetime and counter-ion selectivity[36]. Ion exchange membranes often exhibit a trade-off between conductivity and selectivity. Specifically for BPM-based $CO_2$ electrolysis, the conductivity and water dissociation kinetics of commercial BPMs should mainly be improved.

To improve conductivity and water permeability, the most straightforward method is to decrease the membrane thickness. Highly conductive polymers with sufficient mechanical stability for an ultrathin (<30 µm), self-standing layer already exist for the individual polymers (for example, the perfluorinated, sulfonic acid-based Nafion for CEMs and quaternary ammonium-based polymers (such as Orion and PiperION) for AEMs). Compatible chemistries with similar swelling degrees must be found for a stable BPM with a long lifetime. Additionally, since water can be most easily supplied from the anolyte, and some AEMs (such as PiperION) have a low water permeability[37], an asymmetric BPM with a thin AEL is a logical design strategy. Although decreasing the thickness will increase co-ion crossover, we argue that a minor amount of cation crossover from the anolyte could actually be beneficial for the performance of the system[38], or it could be tuned by using larger cations. Moreover, crossover of (bi)carbonates will probably be irrelevant at high current densities (>1 A) due to the electro-osmotic drag in the opposite direction[39].

Simultaneously increasing both the conductivity and the selectivity of ion exchange membranes is a widely known challenge, but it is a progressing field. Kitto and Kamcev[40] are working on increasing the charge density by placing the charged functional groups in the polymeric backbone itself, to remove trade-off of cross-linking versus functionality. Other promising methods to increase the conductivity include the alignment of the polymeric chains in order to optimize ionic pathway; for example, by conducting the polymerization under an electric field[41].

Solutions for enhanced water dissociation kinetics include three-dimensional (3D) interfaces and water dissociation catalysts blended between the layers. A 3D interface can be created by, for example, electrospinning the two ionomers simultaneously, which increases the contact area and improves the adhesion between the layers[42,43]. A catalyst blended in the interfacial layer enhances the kinetics of water dissociation and has been shown to largely decrease the ohmic resistance of BPMs[44]. Understanding of the catalysis mechanism with respect to the application can contribute to the design of these interfacial catalyst layers[33,45,46], as the catalyst criteria could differ for water dissociation, water recombination and carbonate recombination.

The use of graphene oxide and thin layers has demonstrated stable low overpotentials (<250 mV at 1 A $cm^2$), and strongly asymmetric BPMs have even reached 9 A $cm^2$ (refs. 47,48), surpassing the 600 mA $cm^2$ limiting current of existing commercial BPMs.

In summary, we argue that avoiding $CO_2$ crossover and ensuring favourable anode conditions are crucial steps towards the scale-up of $CO_2$ electrolysis. Reverse-bias BPMs provide these conditions for a stable and scalable process, but improvements are needed in the cathode interaction and water dissociation efficiency. We have shown that the Faradaic efficiency can be improved when the acidic $CO_2R$ catalyst interfaces and proton mobility are controlled: five strategies are available for that. When also implementing thickness optimization, 3D interfaces with new water dissociation catalysts and available conductive polymers, the reverse-bias BPM system has high potential as the primary choice of separator for stable and scalable $CO_2$ electrolysis.

## Data availability

Source data are provided with this paper.

## References


1. Salvatore, D. A. et al. Designing anion exchange membranes for $CO_2$ electrolysers. *Nat. Energy* **6**, 339–348 (2021).
2. Vass, Á. et al. Local chemical environment governs anode processes in $CO_2$ electrolyzers. *ACS Energy Lett.* **6**, 3801–3808 (2021).
3. Minke, C., Suermann, M., Bensmann, B. & Hanke-Rauschenbach, R. Is iridium demand a potential bottleneck in the realization of large-scale PEM water electrolysis? *Int. J. Hydrog. Energy* **46**, 23581–23590 (2021).
4. Rabinowitz, J. A. & Kanan, M. W. The future of low-temperature carbon dioxide electrolysis depends on solving one basic problem. *Nat. Commun.* **11**, 5231 (2020).
5. Sharifian, R., Wagterveld, R. M., Digdaya, I. A., Xiang, C. & Vermaas, D. A. Electrochemical carbon dioxide capture to close the carbon cycle. *Energy Environ. Sci.* **14**, 781–814 (2021).
6. McQueen, N. et al. A review of direct air capture (DAC): scaling up commercial technologies and innovating for the future. *Prog. Energy* **3**, 032001 (2021).
7. Xie, X. et al. Oxygen evolution reaction in alkaline environment: material challenges and solutions. *Adv. Funct. Mater.* **32**, 2110036 (2022).
8. Kim, B., Ma, S., Molly Jhong, H.-R. & Kenis, P. J. A. Influence of dilute feed and pH on electrochemical reduction of $CO_2$ to CO on Ag in a continuous flow electrolyzer. *Electrochim. Acta* **166**, 271–276 (2015).
9. Monteiro, M. C. O., Philips, M. F., Schouten, K. J. P. & Koper, M. T. M. Efficiency and selectivity of $CO_2$ reduction to CO on gold gas diffusion electrodes in acidic media. *Nat. Commun.* **12**, 4943 (2021).
10. Erick, H. J. et al. $CO_2$ electrolysis to multicarbon products in strong acid. *Science* **372**, 1074–1078 (2021).
11. Bondue, C. J., Graf, M., Goyal, A. & Koper, M. T. M. Suppression of hydrogen evolution in acidic electrolytes by electrochemical $CO_2$ reduction. *J. Am. Chem. Soc.* **143**, 279–285 (2021).
12. O'Brien, C. P. et al. Single pass $CO_2$ conversion exceeding 85% in the electrosynthesis of multicarbon products via local $CO_2$ regeneration. *ACS Energy Lett.* **6**, 2952–2959 (2021).
13. Xie, K. et al. Bipolar membrane electrolyzers enable high single-pass $CO_2$ electroreduction to multicarbon products. *Nat. Commun.* **13**, 3609 (2022).
14. Eriksson, B. et al. Mitigation of carbon crossover in $CO_2$ electrolysis by use of bipolar membranes. *J. Electrochem. Soc.* **169**, 034508 (2022).
15. Aydogan Gokturk, P. et al. The Donnan potential revealed. *Nat. Commun.* **13**, 5880 (2022).
16. Pärnamäe, R. et al. Bipolar membranes: a review on principles, latest developments, and applications. *J. Memb. Sci.* **617**, 118538 (2021).
17. Blommaert, M. A., Verdonk, J. A. H., Blommaert, H. C. B., Smith, W. A. & Vermaas, D. A. Reduced ion crossover in bipolar membrane electrolysis via increased current density, molecular size, and valence. *ACS Appl. Energy Mater.* **3**, 5804–5812 (2020).
18. Li, Y. C. et al. Bipolar membranes inhibit product crossover in $CO_2$ electrolysis cells. *Adv. Sustain. Syst.* **2**, 1700187 (2018).
19. Disch, J., Ingenhoven, S. & Vierrath, S. Bipolar membrane with porous anion exchange layer for efficient and long-term stable electrochemical reduction of $CO_2$ to CO. *Adv. Energy Mater.* **13**, 2301614 (2023).
20. Subramanian, S., Middelkoop, J. & Burdyny, T. Spatial reactant distribution in $CO_2$ electrolysis: balancing $CO_2$ utilization and faradaic efficiency. *Sustain. Energy Fuels* **5**, 6040–6048 (2021).
21. Liu, X., Monteiro, M. C. O. & Koper, M. T. M. Interfacial pH measurements during $CO_2$ reduction on gold using a rotating ring-disk electrode. *Phys. Chem. Chem. Phys.* **25**, 2897–2906 (2023).
22. Bui, J. C. et al. Analysis of bipolar membranes for electrochemical $CO_2$ capture from air and oceanwater. *Energy Environ. Sci.* **16**, 5076–5095 (2023).
23. Toh, W. L., Dinh, H. Q., Chu, A. T., Sauvé, E. R. & Surendranath, Y. The role of ionic blockades in controlling the efficiency of energy recovery in forward bias bipolar membranes. *Nat. Energy* **8**, 1405–1416 (2023).
24. Dinh, H. Q., Toh, W. L., Chu, A. T. & Surendranath, Y. Neutralization short-circuiting with weak electrolytes erodes the efficiency of bipolar membranes. *ACS Appl. Mater. Interfaces* **15**, 4001–4010 (2023).
25. Petrov, K. V. et al. Anion-exchange membranes with internal microchannels for water control in $CO_2$ electrolysis. *Sustain. Energy Fuels* **6**, 5077–5088 (2022).
26. Xu, Y. et al. A microchanneled solid electrolyte for carbon-efficient $CO_2$ electrolysis. *Joule* **6**, 1333–1343 (2022).
27. Kim, J. Y. 'T. ' et al. Recovering carbon losses in $CO_2$ electrolysis using a solid electrolyte reactor. *Nat. Catal.* **5**, 288–299 (2022).
28. Monteiro, M. C. O. et al. Absence of $CO_2$ electroreduction on copper, gold and silver electrodes without metal cations in solution. *Nat. Catal.* **4**, 654–662 (2021).
29. Birdja, Y. Y. et al. Advances and challenges in understanding the electrocatalytic conversion of carbon dioxide to fuels. *Nat. Energy* **4**, 732–745 (2019).
30. Xiao, T. et al. Proton antagonist membrane towards exclusive $CO_2$ reduction. *Nano Res.* **16**, 4589–4595 (2023).
31. Siritanaratkul, B. et al. Zero-gap bipolar membrane electrolyzer for carbon dioxide reduction using acid-tolerant molecular electrocatalysts. *J. Am. Chem. Soc.* **144**, 7551–7556 (2022).
32. Guo, J. et al. Direct seawater electrolysis by adjusting the local reaction environment of a catalyst. *Nat. Energy* **8**, 264–272 (2023).
33. Yan, Z., Hitt, J. L., Zeng, Z., Hickner, M. A. & Mallouk, T. E. Improving the efficiency of $CO_2$ electrolysis by using a bipolar membrane with a weak-acid cation exchange layer. *Nat. Chem.* **13**, 33–40 (2021).
34. Endrődi, B. et al. Operando cathode activation with alkali metal cations for high current density operation of water-fed zero-gap carbon dioxide electrolysers. *Nat. Energy* **6**, 439–448 (2021).
35. Baumgartner, L. M., Koopman, C. I., Forner-Cuenca, A. & Vermaas, D. A. Narrow pressure stability window of gas diffusion electrodes limits the scale-up of $CO_2$ electrolyzers. *ACS Sustain. Chem. Eng.* **10**, 4683–4693 (2022).
36. Blommaert, M. A. et al. Insights and challenges for applying bipolar membranes in advanced electrochemical energy systems. *ACS Energy Lett.* **6**, 2539–2548 (2021).

37. Khalid, H., Najibah, M., Park, H. S., Bae, C. & Henkensmeier, D. Properties of anion exchange membranes with a focus on water electrolysis. *Membranes (Basel)* **12**, 989 (2022).
38. Liu, Z., Yang, H., Kutz, R. & Masel, R. I. $CO_2$ electrolysis to CO and $O_2$ at high selectivity, stability and efficiency using sustainion membranes. *J. Electrochem. Soc.* **165**, J3371–J3377 (2018).
39. Yang, K. et al. Cation-driven increases of $CO_2$ utilization in a bipolar membrane electrode assembly for $CO_2$ electrolysis. *ACS Energy Lett.* **6**, 4291–4298 (2021).
40. Kitto, D. & Kamcev, J. The need for ion-exchange membranes with high charge densities. *J. Membr. Sci.* **677**, 121608 (2023).
41. Hyun, J. et al. Magnetic field-induced through-plane alignment of the proton highway in a proton exchange membrane. *ACS Appl. Energy Mater.* **3**, 4619–4628 (2020).
42. Powers, D. et al. Freestanding bipolar membranes with an electrospun junction for high current density water splitting. *ACS Appl. Mater. Interfaces* **14**, 36092–36104 (2022).
43. Xu, Z. et al. Continuous ammonia electrosynthesis using physically interlocked bipolar membrane at 1000 mA $cm^{-2}$. *Nat. Commun.* **14**, 1619 (2023).
44. Chen, Y. et al. High-performance bipolar membrane development for improved water dissociation. *ACS Appl. Polym. Mater.* **2**, 4559–4569 (2020).
45. Mitchell, J. B., Chen, L., Langworthy, K., Fabrizio, K. & Boettcher, S. W. Catalytic proton–hydroxide recombination for forward-bias bipolar membranes. *ACS Energy Lett.* **7**, 3967–3973 (2022).
46. Chen, L., Xu, Q. & Boettcher, S. W. Kinetics and mechanism of heterogeneous voltage-driven water-dissociation catalysis. *Joule* **7**, 1867–1886 (2023).
47. Lucas, É. et al. Asymmetric bipolar membrane for high current density electrodialysis operation with exceptional stability. Preprint at *ChemRxiv* https://doi.org/10.26434/chemrxiv-2023-n4c6x (2023).
48. Mayerhöfer, B. et al. Bipolar membrane electrode assemblies for water electrolysis. *ACS Appl. Energy Mater.* **3**, 9635–9644 (2020).
49. Mardle, P., Cassegrain, S., Habibzadeh, F., Shi, Z. & Holdcroft, S. Carbonate ion crossover in zero-gap, KOH anolyte $CO_2$ electrolysis. *J. Phys. Chem. C* **125**, 25446–25454 (2021).
50. Blommaert, M. A., Subramanian, S., Yang, K., Smith, W. A. & Vermaas, D. A. High indirect energy consumption in AEM-based $CO_2$ electrolyzers demonstrates the potential of bipolar membranes. *ACS Appl. Mater. Interfaces* **14**, 557–563 (2022).
51. Larrazábal, G. O. et al. Analysis of mass flows and membrane cross-over in $CO_2$ reduction at high current densities in an MEA-type electrolyzer. *ACS Appl. Mater. Interfaces* **11**, 41281–41288 (2019).
52. Endrődi, B. et al. High carbonate ion conductance of a robust PiperION membrane allows industrial current density and conversion in a zero-gap carbon dioxide electrolyzer cell. *Energy Environ. Sci.* **13**, 4098–4105 (2020).
53. Jeng, E. & Jiao, F. Investigation of $CO_2$ single-pass conversion in a flow electrolyzer. *React. Chem. Eng.* **5**, 1768–1775 (2020).
54. Ma, M. et al. Insights into the carbon balance for $CO_2$ electroreduction on Cu using gas diffusion electrode reactor designs. *Energy Environ. Sci.* **13**, 977–985 (2020).
55. Ma, M., Kim, S., Chorkendorff, I. & Seger, B. Role of ion-selective membranes in the carbon balance for $CO_2$ electroreduction via gas diffusion electrode reactor designs. *Chem. Sci.* **11**, 8854–8861 (2020).
56. Hansen, K. U., Cherniack, L. H. & Jiao, F. Voltage loss diagnosis in $CO_2$ electrolyzers using five-electrode technique. *ACS Energy Lett.* **7**, 4504–4511 (2022).
57. Khan, M. A. et al. Zero-crossover electrochemical $CO_2$ reduction to ethylene with co-production of valuable chemicals. *Chem. Catal.* **2**, 2077–2095 (2022).
58. Jeanty, P. et al. Upscaling and continuous operation of electrochemical $CO_2$ to CO conversion in aqueous solutions on silver gas diffusion electrodes. *J. CO2 Util.* **24**, 454–462 (2018).
59. Del Castillo, A. et al. Sn nanoparticles on gas diffusion electrodes: synthesis, characterization and use for continuous $CO_2$ electroreduction to formate. *J. CO2 Util.* **18**, 222–228 (2017).
60. Vennekoetter, J.-B., Sengpiel, R. & Wessling, M. Beyond the catalyst: how electrode and reactor design determine the product spectrum during electrochemical $CO_2$ reduction. *Chem. Eng. J.* **364**, 89–101 (2019).


## Acknowledgements

This work is part of the research programme Towards Large-Scale Electroconversion Systems financed by Shell and the top sectors Chemistry, High Tech Systems and Materials and Energy. This project has received funding from the European Research Council under the European Union's Horizon 2020 research and innovation programme (grant agreement 852115). This work reflects the authors' views and the European Research Council Executive Agency is not responsible for any use resulting from the information it contains.

## Competing interests

The authors declare no competing interests.

## Additional information

**Supplementary information** The online version contains supplementary material available at https://doi.org/10.1038/s41560-024-01574-y.

**Correspondence and requests for materials** should be addressed to Marc T. M. Koper, Thomas Burdyny or David A. Vermaas.

**Peer review information** *Nature Energy* thanks Amitava Sarkar and the other, anonymous, reviewer(s) for their contribution to the peer review of this work.